



# Comprehensive characterization of a general composite waveplate by spectroscopic Mueller matrix polarimetry

HONGGANG GU,<sup>1</sup> XIUGUO CHEN,<sup>1,2</sup> YATING SHI,<sup>1</sup> HAO JIANG,<sup>1</sup> CHUANWEI ZHANG,<sup>1</sup> PENG GONG,<sup>1</sup> AND SHIYUAN LIU<sup>1,3</sup>

<sup>1</sup>*State Key Laboratory of Digital Manufacturing Equipment and Technology, Huazhong University of Science and Technology, Wuhan, Hubei 430074, China*

<sup>2</sup>*xiuguo@hust.edu.cn*

<sup>3</sup>*shyliu@hust.edu.cn*

**Abstract:** Composite waveplates (CWs) consisting of multiple single waveplates are basic polarization elements and widely used to manipulate the polarized light in optical systems, and their performances affect the final accuracy and precision significantly. This research proposes a method for the comprehensive characterization of an arbitrary CW based on spectroscopic Mueller matrix polarimetry. An analytical model is established to describe a general CW by extending Jones' equivalent theorem with Mueller matrix calculus. In this model, an arbitrary CW is optically equivalent to a cascaded system consisting of a linear retarder with slight diattenuation followed by an optical rotator, and its polarization properties are completely described by four polarization parameters, including the retardance, the fast axis azimuth, the rotation angle, and the diattenuation angle. Analytical relations between the polarization properties, the structure, and the Mueller matrix of the CW are then derived from the established model. By the proposed method, the polarization parameters of an arbitrary CW can be comprehensively characterized over an ultra-wide spectral range via only one measurement. Moreover, the actual structure of the CW, including the thicknesses and fast axis azimuths of the single waveplates, as well as the axis alignment errors, can be completely reconstructed from the polarization spectra. Experiments performed with a house-developed broadband Mueller matrix polarimeter on three typical CWs including a compound zero-order waveplate, an achromatic waveplate and a specially designed biplate have demonstrated the capability of the proposed method.

© 2018 Optical Society of America under the terms of the [OSA Open Access Publishing Agreement](#)

**OCIS codes:** (120.0120) Instrumentation, measurement, and metrology; (120.2130) Ellipsometry and polarimetry; (230.5440) Polarization-selective devices; (260.5430) Polarization; (120.6200) Spectrometers and spectroscopic instrumentation.

## References and links

1. T. Mu, C. Zhang, Q. Li, and R. Liang, "Achromatization of waveplate for broadband polarimetric system," *Opt. Lett.* **40**(11), 2485–2488 (2015).
2. H. Gu, X. Chen, H. Jiang, C. Zhang, and S. Liu, "Optimal broadband Mueller matrix ellipsometer using multi-waveplates with flexibly oriented axes," *J. Opt.* **18**(2), 025702 (2016).
3. L. Liu, A. Zeng, L. Zhu, and H. Huang, "Lateral shearing interferometer with variable shearing for measurement of a small beam," *Opt. Lett.* **39**(7), 1992–1995 (2014).
4. S. L. Danilishin, E. Knyazev, N. V. Voronchev, F. Y. Khalili, C. Graf, S. Steinlechner, J. S. Hennig, and S. Hild, "A new quantum speed-meter interferometer: measuring speed to search for intermediate mass black holes," *Light Sci. Appl.* **7**(1), 11 (2018).
5. Y. Qu, L. Li, Y. Shen, X. Wei, T. T. W. Wong, P. Hu, J. Yao, K. Maslov, and L. V. Wang, "Dichroism-sensitive photoacoustic computed tomography," *Optica* **5**(4), 495–500 (2018).
6. D. S. Naik, C. G. Peterson, A. G. White, A. J. Berglund, and P. G. Kwiat, "Entangled state quantum cryptography: eavesdropping on the ekert protocol," *Phys. Rev. Lett.* **84**(20), 4733–4736 (2000).
7. J. Li, Y. Tan, and S. Zhang, "Generation of phase difference between self-mixing signals in a-cut Nd:YVO<sub>4</sub> laser with a waveplate in the external cavity," *Opt. Lett.* **40**(15), 3615–3618 (2015).
8. J. L. Vilas and A. Lazarova-Lazarova, "A simple analytical method to obtain achromatic waveplate retarders," *J. Opt.* **19**(4), 045701 (2017).

9. A. A. Rangelov and E. Kyoseva, "Broadband composite polarization rotator," *Opt. Commun.* **338**, 574–577 (2015).
10. X. Tu, L. Jiang, M. Ibn-Elhaj, and S. Pau, "Design, fabrication and testing of achromatic elliptical polarizer," *Opt. Express* **25**(9), 10355–10367 (2017).
11. H. Hurwitz, Jr. and R. C. Jones, "A new calculus for the treatment of optical systems. Part II. Proof of three general equivalence theorems," *J. Opt. Soc. Am.* **31**(7), 493–499 (1941).
12. D. B. Chenault and R. A. Chipman, "Measurements of linear diattenuation and linear retardance spectra with a rotating sample spectropolarimeter," *Appl. Opt.* **32**(19), 3513–3519 (1993).
13. L. Broch, A. En Naciri, and L. Johann, "Systematic errors for a Mueller matrix dual rotating compensator ellipsometer," *Opt. Express* **16**(12), 8814–8824 (2008).
14. E. A. West and M. H. Smith, "Polarization errors associated with birefringent waveplates," *Opt. Eng.* **34**(6), 1574–1580 (1995).
15. B. Boulbry, B. Bousquet, B. Le Jeune, Y. Guern, and J. Lotrian, "Polarization errors associated with zero-order achromatic quarter-wave plates in the whole visible spectral range," *Opt. Express* **9**(5), 225–235 (2001).
16. H. Dong, M. Tang, and Y. Gong, "Measurement errors induced by deformation of optical axes of achromatic waveplate retarders in RRFP Stokes polarimeters," *Opt. Express* **20**(24), 26649–26666 (2012).
17. P. Zhang, Y. Tan, W. Liu, and W. Chen, "Methods for optical phase retardation measurement: A review," *Sci. China Technol. Sci.* **56**(5), 1155–1163 (2013).
18. L. Yao, Z. Zhiyao, and W. Runwen, "Optical heterodyne measurement of the phase retardation of a quarter-wave plate," *Opt. Lett.* **13**(7), 553–555 (1988).
19. C. Chou, Y. C. Huang, and M. Chang, "Effect of elliptical birefringence on the measurement of the phase retardation of a quartz wave plate by an optical heterodyne polarimeter," *J. Opt. Soc. Am. A* **14**(6), 1367–1372 (1997).
20. C. J. Yu, C. E. Lin, Y. C. Li, L. D. Chou, J. S. Wu, C. C. Lee, and C. Chou, "Dual-frequency heterodyne ellipsometer for characterizing generalized elliptically birefringent media," *Opt. Express* **17**(21), 19213–19224 (2009).
21. Y. L. Lo, C. H. Lai, J. F. Lin, and P. F. Hsu, "Simultaneous absolute measurements of principal angle and phase retardation with a new common-path heterodyne interferometer," *Appl. Opt.* **43**(10), 2013–2022 (2004).
22. Y. T. Jeng and Y. L. Lo, "Heterodyne polariscope for sequential measurements of the complete optical parameters of a multiple-order wave plate," *Appl. Opt.* **45**(6), 1134–1141 (2006).
23. C. C. Chou, S. Y. Lu, T. Lin, S. H. Lu, and R. J. Jeng, "Environment-noise-free optical heterodyne retardation measurement using a double-pass acousto-optic frequency shifter," *Opt. Lett.* **41**(22), 5138–5141 (2016).
24. W. Liu, M. Liu, and S. Zhang, "Method for the measurement of phase retardation of any wave plate with high precision," *Appl. Opt.* **47**(30), 5562–5569 (2008).
25. W. Chen, H. Li, S. Zhang, and X. Long, "Measurement of phase retardation of waveplate online based on laser feedback," *Rev. Sci. Instrum.* **83**(1), 013101 (2012).
26. W. Chen, S. Zhang, and X. Long, "Optic axis determination based on polarization flipping effect induced by optical feedback," *Opt. Lett.* **38**(7), 1080–1082 (2013).
27. P. A. Williams, A. H. Rose, and C. M. Wang, "Rotating-polarizer polarimeter for accurate retardance measurement," *Appl. Opt.* **36**(25), 6466–6472 (1997).
28. P. C. Chen, Y. L. Lo, T. C. Yu, J. F. Lin, and T. T. Yang, "Measurement of linear birefringence and diattenuation properties of optical samples using polarimeter and Stokes parameters," *Opt. Express* **17**(18), 15860–15884 (2009).
29. J. F. Lin and Y. L. Lo, "Measurement of optical rotation and phase retardance of optical samples with depolarization effects using linearly and circularly polarized probe lights," *Opt. Lasers Eng.* **47**(9), 948–955 (2009).
30. C. C. Liao and Y. L. Lo, "Extraction of anisotropic parameters of turbid media using hybrid model comprising differential- and decomposition-based Mueller matrices," *Opt. Express* **21**(14), 16831–16853 (2013).
31. J. A. J. Fells, S. J. Elston, M. J. Booth, and S. M. Morris, "Time-resolved retardance and optic-axis angle measurement system for characterization of flexoelectro-optic liquid crystal and other birefringent devices," *Opt. Express* **26**(5), 6126–6142 (2018).
32. X. Chen, L. Yan, and X. S. Yao, "Waveplate analyzer using binary magneto-optic rotators," *Opt. Express* **15**(20), 12989–12994 (2007).
33. J. B. Masson and G. Gallot, "Terahertz achromatic quarter-wave plate," *Opt. Lett.* **31**(2), 265–267 (2006).
34. J. Liu, Y. Cai, H. Chen, X. Zeng, D. Zou, and S. Xu, "Design for the optical retardation in broadband zero-order half-wave plates," *Opt. Express* **19**(9), 8557–8564 (2011).
35. J. M. Herrera-Fernandez, J. L. Vilas, L. M. Sanchez-Brea, and E. Bernabeu, "Design of superachromatic quarter-wave retarders in a broad spectral range," *Appl. Opt.* **54**(33), 9758–9762 (2015).
36. S. Liu, X. Chen, and C. Zhang, "Development of a broadband Mueller matrix ellipsometer as a powerful tool for nanostructure metrology," *Thin Solid Films* **584**, 176–185 (2015).
37. S. Y. Lu and R. A. Chipman, "Interpretation of Mueller matrices based on polar decomposition," *J. Opt. Soc. Am. A* **13**(5), 1106–1113 (1996).
38. R. Ossikovski, "Differential matrix formalism for depolarizing anisotropic media," *Opt. Lett.* **36**(12), 2330–2332 (2011).

39. J. Humlicek, "Polarized light and ellipsometry," in *Handbook of ellipsometry*, H. G. Tompkins, and E. A. Irene, eds. (William Andrew, 2005), Chap. 1, pp. 59–66.
40. D. Clarke, "Interference effects in compound and achromatic wave plates," *J. Opt. A, Pure Appl. Opt.* **6**(11), 1041–1046 (2004).
41. J. Lee, P. I. Rovira, I. An, and R. W. Collins, "Alignment and calibration of the MgF<sub>2</sub> biplate compensator for applications in rotating-compensator multichannel ellipsometry," *J. Opt. Soc. Am. A* **18**(8), 1980–1985 (2001).
42. J. M. Beckers, "Achromatic linear retarders," *Appl. Opt.* **10**(4), 973–975 (1971).
43. X. Chen, C. Zhang, and S. Liu, "Depolarization effects from nanoimprinted grating structures as measured by Mueller matrix polarimetry," *Appl. Phys. Lett.* **103**(15), 151605 (2013).
44. H. Gu, S. Liu, X. Chen, and C. Zhang, "Calibration of misalignment errors in composite waveplates using Mueller matrix ellipsometry," *Appl. Opt.* **54**(4), 684–693 (2015).
45. H. Gu, X. Chen, H. Jiang, C. Zhang, W. Li, and S. Liu, "Accurate alignment of optical axes of a biplate using a spectroscopic Mueller matrix ellipsometer," *Appl. Opt.* **55**(15), 3935–3941 (2016).
46. Q. Zheng, Z. Han, and L. Chen, "Determination of the misalignment error of a compound zero-order waveplate using the spectroscopic phase shifting method," *Opt. Commun.* **374**, 18–23 (2016).
47. Z. Han and Q. Zheng, "Self-spectral calibration of a compound zero-order waveplate at blind rotation angles," *Opt. Lasers Eng.* **91**, 257–260 (2017).
48. D. K. Aitken and J. H. Hough, "Spectral modulation, or ripple, in retardation plates for linear and circular polarization," *Publ. Astron. Soc. Pac.* **113**(788), 1300–1305 (2001).
49. X. Chen, S. Liu, H. Gu, and C. Zhang, "Formulation of error propagation and estimation in grating reconstruction by a dual-rotating compensator Mueller matrix polarimeter," *Thin Solid Films* **571**, 653–659 (2014).
50. S. Chandrasekhar, "The dispersion and thermo-optic behaviour of vitreous silica," *Proc. Indian Acad. Sci. A* **34**, 275–282 (1951).
51. M. J. Dodge, "Refractive properties of magnesium fluoride," *Appl. Opt.* **23**(12), 1980–1985 (1984).

## 1. Introduction

Waveplates made of birefringent materials are basic polarization elements and widely used in optical systems, such as ellipsometry/polarimetry [1,2], interferometry [3,4], tomography [5], cryptography [6] and laser systems [7], to control and manipulate the polarization states of a polarized light. A composite waveplate (CW) consisting of multiple single waveplates can be specially designed and applied as a linear retarder [8], an optical rotator (namely a circular retarder) [9], an elliptical retarder [2], or an elliptical polarizer [10] in the systems. According to Jones' theorem, a general CW can be optically equivalent to a linear retarder and a rotator, and described by three equivalent polarization parameters, i.e., the retardance, the fast axis azimuth, and the rotation angle [11]. In practice, a CW invariably contains some linear diattenuation due to the dichroic artifacts or the interference effect resulting from the multi-reflections between the plate planes [12]. Thus, a comprehensive characterization of the polarization properties of a practical CW requires four polarization parameters including the (linear) retardance, the fast axis azimuth, the rotation angle (i.e., the circular retardance), and the diattenuation angle. Polarization errors associated with these parameters, such as the retardance deviations, the axis alignment errors, the field-of-view effect, and the dichroic artifacts, will significantly degrade the final performances of the systems [13–16]. On the other hand, the polarization properties and their corresponding errors are closely related to the structure of the CW, including the thicknesses and the layout of the component single waveplates, and the intersection angles among the fast axes and the axis alignment [1,2,8–10]. Errors in the structure parameters from the manufacturing or the installation procedures, such as the thickness deviation, the axis misalignment, and the axis tilt error, will result in deviations and oscillations in the polarization parameters of the CW [14–16]. Therefore, it is of great importance to comprehensively characterize the polarization properties as well as the actual structure of a CW for both the manufacturing process and the applications.

Various methods and techniques have been developed to characterize birefringent waveplates as reviewed by Zhang *et al.* [17]. Here, we recall and summarize several typical techniques among numerous excellent works. The optical heterodyne technique is a typically used method for the characterization of a waveplate [18–23]. However, the conventional heterodyne method based on the common-path interferometric technique can only obtain the linear retardance of a waveplate [18]. By introducing polarimetric techniques into the

conventional optical heterodyne interferometer, Chou *et al.* studied the elliptical retardance (combination of linear retardance and circular retardance) of optically active waveplates [19,20], and Lo *et al.* simultaneously measured the principal axis angle and the phase retardance of different waveplates [21,22]. Recently, an environment-noise-free optical heterodyne interferometer was proposed to measure the phase retardance of waveplates with immunity to environment instability [23]. Zhang and his team developed a series of laser-based techniques including the laser frequency-splitting method, the laser feedback method, and the polarization flipping method, and they applied these systems to characterize waveplates with very high precision and accuracy [17,24–26]. The polarimetry is another commonly used technique, and different types of polarimeters have been developed to characterize the polarization properties of waveplates [12,27–32]. Chenault and Chipman applied a rotating sample spectropolarimeter to measure the linear retardance and linear diattenuation of a quasi-achromatic waveplate [12]. Williams described a precise measurement of the retardance using a rotating-polarizer polarimeter [27]. Lo and Lin *et al.* used the Stokes polarimeter and the Stokes-Mueller matrix formalism and characterized the polarization properties of different anisotropic samples [28–30]. Very recently, a time-resolved polarimeter has been developed to characterize the retardance and the optic axis angle of birefringent devices [31]. In summary, the above-mentioned techniques can only characterize part of the four required polarization parameters (usually the retardance, the fast axis azimuth, and/or the rotation angle) of some simple waveplates, such as a multi-order single waveplate or a compound zero-order waveplate. Thus, to the best of our knowledge, there is no reported study yet that can achieve a comprehensive characterization of both the polarization properties and the actual structure of a complex CW. In addition, the interferometric and the laser-based techniques are usually performed with a monochromatic source, and need to change sources and other corresponding settings, or additional dispersion equations to evaluate the spectral properties of a waveplate.

Recently, some novel CWs have been designed to meet more critical requirements of broadband, wide-view imaging and high-precision systems [1,2,8–10,33–35]. This brings a big challenge to the existing techniques for the comprehensive characterization of these novel CWs because they may have much more complicate structures and polarization properties. In the meantime, the Mueller matrix polarimeter (MMP, sometimes also called Mueller matrix ellipsometer) has been developed and applied as a powerful tool for the characterization of anisotropic media by providing the  $4 \times 4$  Mueller matrix of the sample in each measurement [36]. Thus, a spectroscopic MMP has the capability and advantages to characterize a general CW which can be treated as a typical transparent anisotropic sample. The main problem lies in that there lacks a suitable model to completely describe the polarization properties and to reconstruct the structure of a general CW with Mueller matrix calculus. The Lu-Chipman decomposition is a traditional method for performing data reduction upon experimentally determined Mueller matrix, which decomposes a Mueller matrix into a sequence of three matrix factors: a diattenuator, followed by a retarder, then followed by a depolarizer [37]. The Lu-Chipman decomposition method can define and compute the diattenuation and the retardance of a Mueller matrix. However, it cannot distinguish the linear retardance (diattenuation) and the circular retardance (diattenuation), and it fails to determine the axis orientation of a polarized elements. Moreover, the sequence order of the matrix factors has great influence on the final decomposition results, and different orders may results in different results. Another commonly used technique for processing the experimental Mueller matrix of a homogeneous anisotropic medium is the differential decomposition method, in which the spatial derivative along the light propagation direction of the Mueller matrix is used to obtain six polarization components, including the linear birefringence/dichroism along the  $x$ - $y$  axes and along the  $\pm 45^\circ$  axes, as well as the circular birefringence/dichroism [38]. However, the differential decomposition method cannot further obtain the retardance/diattenuation from the birefringence/dichroism without the structure information of the medium, such as the

thickness, which cannot be determined by this method. What's more, the axis orientations cannot be determined either from the differential decomposition components. Therefore, the Lu-Chipman decomposition and the differential decomposition are mostly applied to qualitatively analyze the polarization properties of a medium, but can be hardly used to quantitatively determine the polarization parameters and the structure parameters of a CW.

To this end, we propose a method in this paper to comprehensively characterize a general CW using a spectroscopic MMP. An analytical model is constructed to fully describe a general CW by extending Jones' equivalent theorem [11] with Mueller matrix calculus, in which the CW is optically equivalent to a linear retarder with slight diattenuation and a rotator (circular retarder). The polarization properties of the CW are completely described by four equivalent polarization parameters including the (linear) retardance, the fast axis azimuth, the rotation angle (namely the circular retardance) and the diattenuation angle. In the model, relations between the structure parameters, the equivalent polarization parameters, and the Mueller matrix elements of the CW are theoretically derived. By using the proposed method, the polarization properties including all the polarization parameters and the ellipticity of an arbitrary CW can be comprehensively characterized over a wide spectral range through only one measurement. What's more, the actual structures of the CW, including the thicknesses and the fast axis azimuth of the single waveplates, the axis alignment errors, and the global orientation, can be completely reconstructed from the measured spectra. Three typical CWs including a compound zero-order waveplate, an achromatic waveplate and a specially designed biplate were tested by a house-developed broadband MMP as examples. Results and discussions demonstrate the capability and universality of the proposed method.

## 2. Theory

Mueller matrix is often utilized to comprehensively describe the modification properties of a medium on the polarization state of a polarized light [39]. Birefringent waveplate is one of the most commonly used polarization elements to modulate the polarization state by introducing a phase shift between two orthogonal polarization components of the polarized light. Here we consider that the waveplate is arranged in a Cartesian coordinate system, and the light propagates along the  $z$ -axis and perpendicularly to the plate plane.

A single waveplate is usually a slice of birefringent material, and can be treated as a linear retarder. Thus, the Mueller matrix of a single waveplate can be expressed as [39]

$$\mathbf{M}(\delta, \theta) = \mathbf{R}(-\theta)\mathbf{M}(\delta)\mathbf{R}(\theta). \quad (1)$$

where,  $\mathbf{M}(\delta)$  and  $\mathbf{R}(\theta)$  are the intrinsic Mueller matrix of a linear retarder with a linear retardance  $\delta$  and the rotation Mueller matrix with a rotation angle  $\theta$ , and they respectively have the following forms

$$\mathbf{M}(\delta) = \begin{bmatrix} 1 & 0 & 0 & 0 \\ 0 & 1 & 0 & 0 \\ 0 & 0 & \cos \delta & \sin \delta \\ 0 & 0 & -\sin \delta & \cos \delta \end{bmatrix}, \quad (2)$$

$$\mathbf{R}(\theta) = \begin{bmatrix} 1 & 0 & 0 & 0 \\ 0 & \cos(2\theta) & \sin(2\theta) & 0 \\ 0 & -\sin(2\theta) & \cos(2\theta) & 0 \\ 0 & 0 & 0 & 1 \end{bmatrix}, \quad (3)$$

herein,  $\theta$  is the azimuth angle of the fast axis with respect to the  $x$ -axis, and  $\delta$  is the retardance of the waveplate and can be calculated by

$$\delta = \frac{2\pi}{\lambda} d \cdot \Delta n, \quad (4)$$

where  $\Delta n = (n_e - n_o)$  is the birefringence of the material,  $n_e$  and  $n_o$  denote the extraordinary and the ordinary refractive indices,  $d$  and  $\lambda$  refer to the thickness of the waveplate and the vacuum wavelength, respectively.

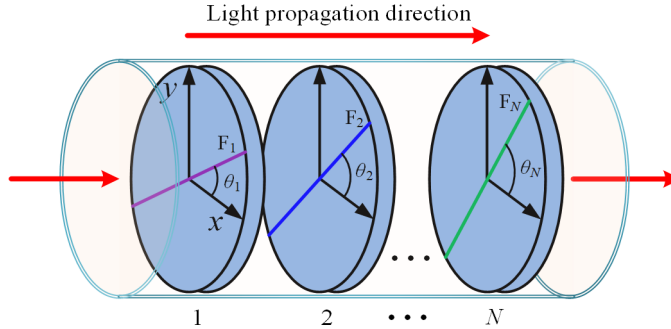


Fig. 1. Schematic of the structure of a general CW.  $F_n$  and  $\theta_n$  ( $n = 1, 2, \dots, N$ ) refer to the fast axis of the  $n$ -th single-waveplate and its azimuth angle with respect to the  $x$ -axis, respectively.

A general CW as schematically shown in Fig. 1 is a stack of single waveplates, whose plate planes are parallel to each other. These single waveplates are numbered as 1, 2, ...,  $N$  in the order of light propagation. Furthermore, let  $d_n$  and  $\theta_n$  denote the thickness and the fast axis azimuth of the  $n$ -th single waveplate, respectively. The retardance of the  $n$ -th single waveplate  $\delta_n$  can be calculated by its thickness according to Eq. (4). According to Jones' theorem, the CW can be optically equivalent to a cascaded system containing a linear retarder and a rotator (also known as a circular retarder) [11].

In general, a waveplate is assumed to have an equal transmittance for the polarized components along the fast axis and the slow axis. However, a practical waveplate invariably exhibits slight linear diattenuation due to the dichroism of the imperfect material or the interference artifacts in the fast axis and slow axis directions resulting from the multi-reflections between the plate planes [12,40]. Here, a polarimetric angle  $\psi$  is introduced to describe the linear diattenuation, which is defined as the ratio of the fast-to-slow-axis transmittance [41],

$$\tan \psi = \frac{t_f}{t_s}, \quad (5)$$

where  $t_f$  and  $t_s$  refer to the amplitude transmission coefficients along the fast axis and the slow axis of the waveplate. Since the diattenuation in a birefringent material usually occurs between the fast axis and the slow axis, the linear retarder and the linear diattenuator are assumed to have the same optic axis, and the combination of them can be regarded as a linear retarder with slight diattenuation, whose polarimetric properties can be described by the following Mueller matrix

$$\mathbf{M}(\delta, \psi) = \begin{bmatrix} 1 & -\cos(2\psi) & 0 & 0 \\ -\cos(2\psi) & 1 & 0 & 0 \\ 0 & 0 & \sin(2\psi)\cos\delta & \sin(2\psi)\sin\delta \\ 0 & 0 & -\sin(2\psi)\sin\delta & \sin(2\psi)\cos\delta \end{bmatrix}. \quad (6)$$

Therefore, a practical CW can be equivalent to a linear retarder, a rotator and a linear diattenuator. In this case, we extend the equivalent theorem to describe a practical CW by taking the diattenuation into account, and the Mueller matrix of the CW can be described as

$$\mathbf{M} = \prod_{n=1}^N \mathbf{M}(\delta_n, \theta_n) \doteq \mathbf{R}(\rho_e) \mathbf{R}(-\theta_e) \mathbf{M}(\delta_e, \psi_e) \mathbf{R}(\theta_e) = \begin{bmatrix} 1 & m_{12} & m_{13} & m_{14} \\ m_{21} & m_{22} & m_{23} & m_{24} \\ m_{31} & m_{32} & m_{33} & m_{34} \\ m_{41} & m_{42} & m_{43} & m_{44} \end{bmatrix}, \quad (7)$$

where,  $m_{ij}$  ( $i, j = 1, 2, 3, 4$ ) refers to the normalized Mueller matrix element of the CW,  $\delta_e$  and  $\psi_e$  are the equivalent retardance of the linear retarder and the equivalent diattenuation angle of the linear diattenuator respectively,  $\theta_e$  is the equivalent fast axis azimuth, and  $\rho_e$  is the equivalent rotation angle (i.e., the circular retardance) of the rotator. The diattenuation angle  $\psi_e$  will constantly equal  $45^\circ$  for an ideal waveplate, but slightly deviate from  $45^\circ$  for a practical waveplate. Specially, in this paper, the counterclockwise is defined as the positive direction for the axis azimuth and rotation angle, conversely the clockwise is defined as the negative direction.

From the above established model, we can see that the Mueller matrix and the equivalent polarization parameters can be totally determined by the structure of the CW including the thicknesses and the fast axis azimuths of the component single waveplates. Expanding Eq. (7), we can derive the relations between the equivalent polarization parameters and the Mueller matrix elements of the CW as given by

$$m_{12} = -C_{\theta_e} C_{\psi_e}, \quad (8a)$$

$$m_{13} = -S_{\theta_e} C_{\psi_e}, \quad (8b)$$

$$m_{14} = m_{41} = 0, \quad (8c)$$

$$m_{21} = -(C_{\theta_e} C_{\rho_e} + S_{\theta_e} S_{\rho_e}) C_{\psi_e}, \quad (8d)$$

$$m_{22} = (C_{\theta_e}^2 + S_{\theta_e}^2 S_{\psi_e} \cos \delta_e) C_{\rho_e} + S_{\theta_e} C_{\theta_e} (1 - S_{\psi_e} \cos \delta_e) S_{\rho_e}, \quad (8e)$$

$$m_{23} = S_{\theta_e} C_{\theta_e} (1 - S_{\psi_e} \cos \delta_e) C_{\rho_e} + (S_{\theta_e}^2 + C_{\theta_e}^2 S_{\psi_e} \cos \delta_e) S_{\rho_e}, \quad (8f)$$

$$m_{24} = (C_{\theta_e} S_{\rho_e} - S_{\theta_e} C_{\rho_e}) S_{\psi_e} \sin \delta_e, \quad (8g)$$

$$m_{31} = (C_{\theta_e} S_{\rho_e} - S_{\theta_e} C_{\rho_e}) C_{\psi_e}, \quad (8h)$$

$$m_{32} = S_{\theta_e} C_{\theta_e} (1 - S_{\psi_e} \cos \delta_e) C_{\rho_e} - (C_{\theta_e}^2 + S_{\theta_e}^2 S_{\psi_e} \cos \delta_e) S_{\rho_e}, \quad (8i)$$

$$m_{33} = (S_{\theta_e}^2 + C_{\theta_e}^2 S_{\psi_e} \cos \delta_e) C_{\rho_e} - S_{\theta_e} C_{\theta_e} (1 - S_{\psi_e} \cos \delta_e) S_{\rho_e}, \quad (8j)$$

$$m_{34} = (S_{\theta_e} S_{\rho_e} + C_{\theta_e} C_{\rho_e}) S_{\psi_e} \sin \delta_e, \quad (8k)$$

$$m_{42} = S_{\theta_e} S_{\psi_e} \sin \delta_e, \quad (8l)$$

$$m_{43} = -C_{\theta_e} S_{\psi_e} \sin \delta_e, \quad (8m)$$

$$m_{44} = S_{\psi_e} \cos \delta_e, \quad (8n)$$

where

$$S_\kappa = \sin(2\kappa), C_\kappa = \cos(2\kappa), (\kappa = \theta_e, \psi_e, \rho_e). \quad (8o)$$

In turn, the polarization parameters of a CW can be resolved from its Mueller matrix. According to Eq. (8), we can obtain various formulas for the polarization parameters in forms of different Mueller matrix elements, and examples are shown as

$$\delta_e = \tan^{-1} \sqrt{\frac{m_{42}^2 + m_{43}^2}{m_{44}^2}}, \quad (9a)$$

$$\theta_e = \frac{1}{2} \tan^{-1} \left( \frac{m_{42}}{m_{43}} \right), \quad (9b)$$

$$\rho_e = \frac{1}{2} \tan^{-1} \left( \frac{m_{23} - m_{32}}{m_{22} + m_{33}} \right), \quad (9c)$$

$$\psi_e = \frac{1}{2} \cos^{-1} \sqrt{m_{12}^2 + m_{13}^2} = \frac{1}{2} \cos^{-1} \sqrt{m_{21}^2 + m_{31}^2}, \quad (9d)$$

Due to the optical activity of the birefringent material and the general structure, a CW will exhibit both linear retardance and circular retardance [15,19,20]. In this case, the CW is an elliptical retarder. In application, people are sometimes concerned about the elliptical features of a CW. Thus, two parameters, namely the elliptical retardance  $\gamma$  and the ellipticity  $\varepsilon$ , are introduced to evaluate the elliptical features of a CW. They are defined by using the linear retardance and the circular retardance of the CW, and given by [20]

$$\gamma = 2 \cos^{-1} \left( \cos \frac{\delta_e}{2} \cos \rho_e \right), \quad (10)$$

$$\varepsilon = \frac{1}{2} \tan^{-1} \left( \cot \frac{\delta_e}{2} \sin \rho_e \right). \quad (11)$$

It should be noted that the specific formulas given by Eq. (9) utilizing several certain Mueller matrix elements may be easily influenced by the measurement noises and errors in the Mueller matrix. To make use of abundant information hidden in the full Mueller matrix and to improve the immunity to errors in the measurement, here we propose a robust solution to more accurately extract the equivalent polarization parameters of a CW from its measured Mueller matrix. This method is essentially an inverse optimization problem, which can be described in a general mathematic form

$$\hat{\mathbf{x}} = \arg \min_{\mathbf{x} \in \Omega} \sum_k \left[ \frac{y_k^c - y_k^m}{\sigma(y_k)} \right]^2, \quad (12)$$

where,  $y_k^c$  and  $y_k^m$  are the theoretically calculated and the measured data respectively,  $\sigma(y_k)$  refers to the estimated standard deviation associated with  $y_k$ ,  $k$  is the index for the data set,  $\mathbf{x}$  and  $\hat{\mathbf{x}}$  refer to the parameters to be determined and the output results for the optimization procedure respectively, and  $\Omega$  is the variable domain for these parameters.

Specific to the extraction for polarization parameters of a CW, the inverse optimization procedure can be described as minimizing the difference between the theoretically calculated Mueller matrix  $\mathbf{M}_c$  and the measured Mueller matrix  $\mathbf{M}_m$  by adjusting the input equivalent

polarization parameters. In this case, we have  $y = m_{ij}$ ,  $\mathbf{x} = [\delta_e, \theta_e, \rho_e, \psi_e]$  and  $\hat{\mathbf{x}} = [\hat{\delta}_e, \hat{\theta}_e, \hat{\psi}_e, \hat{\rho}_e]$  for Eq. (12). The theoretical Mueller matrix of the CW can be calculated according to Eq. (8) by the input equivalent polarization parameters. In practice, the above inverse problem is carried out with a wavelength-by-wavelength regressive iteration procedure by using the Levenberg-Marquardt (LM) algorithm. The initial values of the input parameters for the first wavelength can be calculated from the measured Mueller matrix according to Eq. (9). The output equivalent polarization parameters of the current wavelength are chosen as the initial values of the input parameters of the next wavelength. By repeating this regressive iteration procedure wavelength by wavelength, all the spectra of the equivalent polarization parameters of the CW can be obtained.

Finally, the actual structure of the CW can be determined by fitting the measured spectra of the polarization parameters. This fitting procedure is again an inverse optimization problem, which can be performed by minimizing the difference between the theoretical and the measured spectra by continuously adjusting the input structure parameters. For this procedure, in Eq. (12) the data  $y$  refers to the spectra of the equivalent polarization parameters (i.e.,  $\delta_e(\lambda), \theta_e(\lambda), \rho_e(\lambda)$  and/or  $\psi_e(\lambda)$ ), the parameters to be extracted are structure parameters of the CW, including the thicknesses  $\mathbf{d}$  and the fast axis azimuths  $\boldsymbol{\theta}$  of the single waveplates. The theoretical spectra of the polarization parameters can be calculated by the input structure parameters of the CW according to the model established by Eqs. (1)–(9). With this method, the actual structure of the CW can be completely reconstructed.

### 3. Experiments

#### 3.1 Sample description

In this paper, three CWs of different types are taken as examples to verify the proposed method. For convenience, they are named as CW1, CW2, and CW3, respectively.

- (1) CW1 is a compound zero-order waveplate which is designed as a quarter-wave linear retarder at the central wavelength of 632.8nm made of quartz. It contains two multi-order waveplates whose fast axes are arranged perpendicular to each other. The two multi-order waveplates are mounted in a mechanical bracket with an air-gap between them.
- (2) CW2 is a Bechers' achromatic quarter waveplate [42] for the spectral range of 450–650 nm. It contains three single waveplates, and two of them are made of magnesium fluoride ( $MgF_2$ ), and the third one is made of quartz. The fast axis of the thicker  $MgF_2$  single waveplate is aligned perpendicular to those of the thinner  $MgF_2$  single waveplate and the quartz single waveplate. All the three single waveplates are cemented together with glue and also mounted in a mechanical bracket.
- (3) CW3 is a specific  $MgF_2$  biplate containing two zero-order quarter waveplates (whose central wavelengths are 271 nm and 932 nm respectively) with an intersection angle of 45° between their fast axes. It is specially designed as a polarization modulator for broadband polarimetric systems. The single waveplates are cemented together by the optical cement method without any air gap between them.

For ideal cases, the former two CWs are typical linear retarders, and the last one is a general elliptical retarder. Thus, these three samples can cover most cases of the CWs, and give a comprehensive verification of the proposed method. The structures of the above CWs are specific forms of the schematic shown in Fig. 1. All the waveplate products are supplied in cylindrical mounts engraved with the fast axes of the first single waveplates, which are defined as the global orientations of the CWs. To improve the transmittance, all the waveplates are produced with anti-reflection coatings on both sides. The anti-reflection coatings can also reduce the interference effect between the plate planes of the CWs.

It is worth pointing out that since the thickness of a true zero-order waveplate is only several to tens of micrometers and is too thin to be cut and polished, the component waveplate of the  $MgF_2$  biplate is chosen as a compound zero-order waveplate. And each of them contains two multi-order single waveplates assembled with their optical axes in a crossed position. The effective thicknesses of such a compound zero-order waveplate equals the thickness difference between the two multi-order waveplates. The fast axis azimuth is determined by that of the thicker multi-order single waveplate.

### 3.2 Experimental set-up

In this work, we use a transmission spectroscopic MMP to measure the Mueller matrix of a CW over a wide spectral range as schematically shown in Fig. 2(a). The experimental system contains a broadband light source, a polarization state generator (PSG), a sample stage, a polarization state analyzer (PSA), and a spectrometer. The PSG consists of a linear polarizer followed by a rotating compensator, while the PSA consists of another linear polarizer (named as the analyzer) following a second rotating compensator. The PSG and the PSA can achieve complete polarization modulation and demodulation, and make the ellipsometer capable of measuring the full Mueller matrix of the sample. The CW to be measured is placed on the sample stage between the PSG and the PSA.

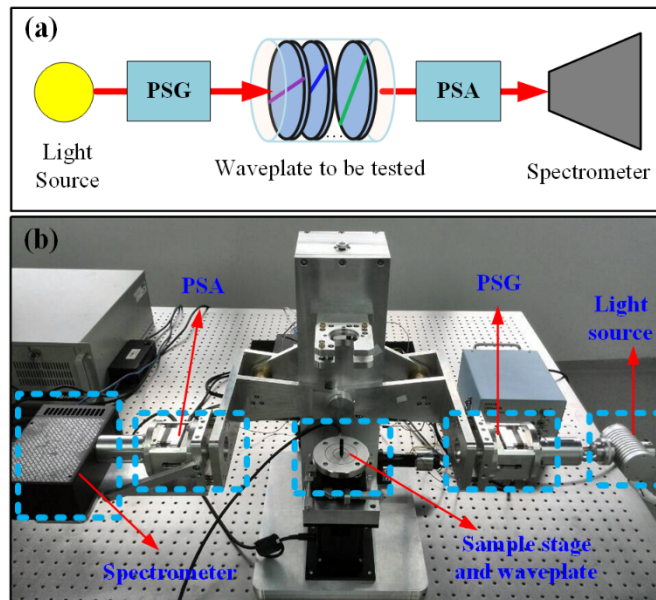


Fig. 2. (a) Schematic of the MMP-based experimental set-up for the characterization of a CW;  
(b) Prototype of the experimental set-up based on a house-developed broadband MMP.

Figure 2(b) shows the prototype of the experimental set-up based on a house-developed broadband MMP [2,36]. The available wavelength range of the house-developed MMP covers 200–1000 nm. Two measurement modes, namely the transmission and the reflective modes, can be chosen by rotating the PSG arm and the PSA arm of the polarimeter simultaneously. In this paper, the CW is measured in the transmission measurement mode. The sample stage is a combination of basic contact slide and rotation stages, which guarantee six degrees of freedom, i.e., horizontal and vertical movement, horizontal tilt adjustment and rotation around the vertical axis.

In the experiments, the waveplate to be tested is first mounted in a scaled turntable placed on the sample stage, and then the sample stage is attentively adjusted to ensure the light spot totally propagates through the waveplate at normal incidence. The global orientation of the

CW can be roughly judged from the tick marks on the turntable and the engraved line on the protecting frame of the CW.

#### 4. Results and discussion

##### 4.1 Mueller matrix measurement

The mentioned CW samples are successively characterized by the house-developed MMP. Since the errors in the instrument may induce significant polarization crosstalk in the final results, the house-developed MMP has been set up with strict system optimization, system calibration and system check to guarantee the precision and accuracy for Mueller matrix measurements. The systematic parameters, including the retardance of the compensator and the azimuths of the polarized elements, have been optimized by a condition number method to improve the immunity of the MMP to these errors. Before measurements, the residual errors and defections in the polarized elements, such as the retardance deviations, the axis azimuth deformations, and the depolarization artifacts, have been calibrated and corrected precisely by using a series of standard SiO<sub>2</sub> thin films. The Mueller matrix measurement precision and accuracy of the house-developed MMP were found to be better than 0.2% and 0.1% respectively. More details about the instrumentation of the house-developed MMP can be referred to our previous work [2].

In the experiment, these CWs are intentionally arranged with arbitrary global orientations to test the effectiveness of the proposed method in the determination of the fast axis azimuths. Based on this consideration, the global orientations of CW1–CW3 are set at around 60°, 0°, and 110°, respectively.

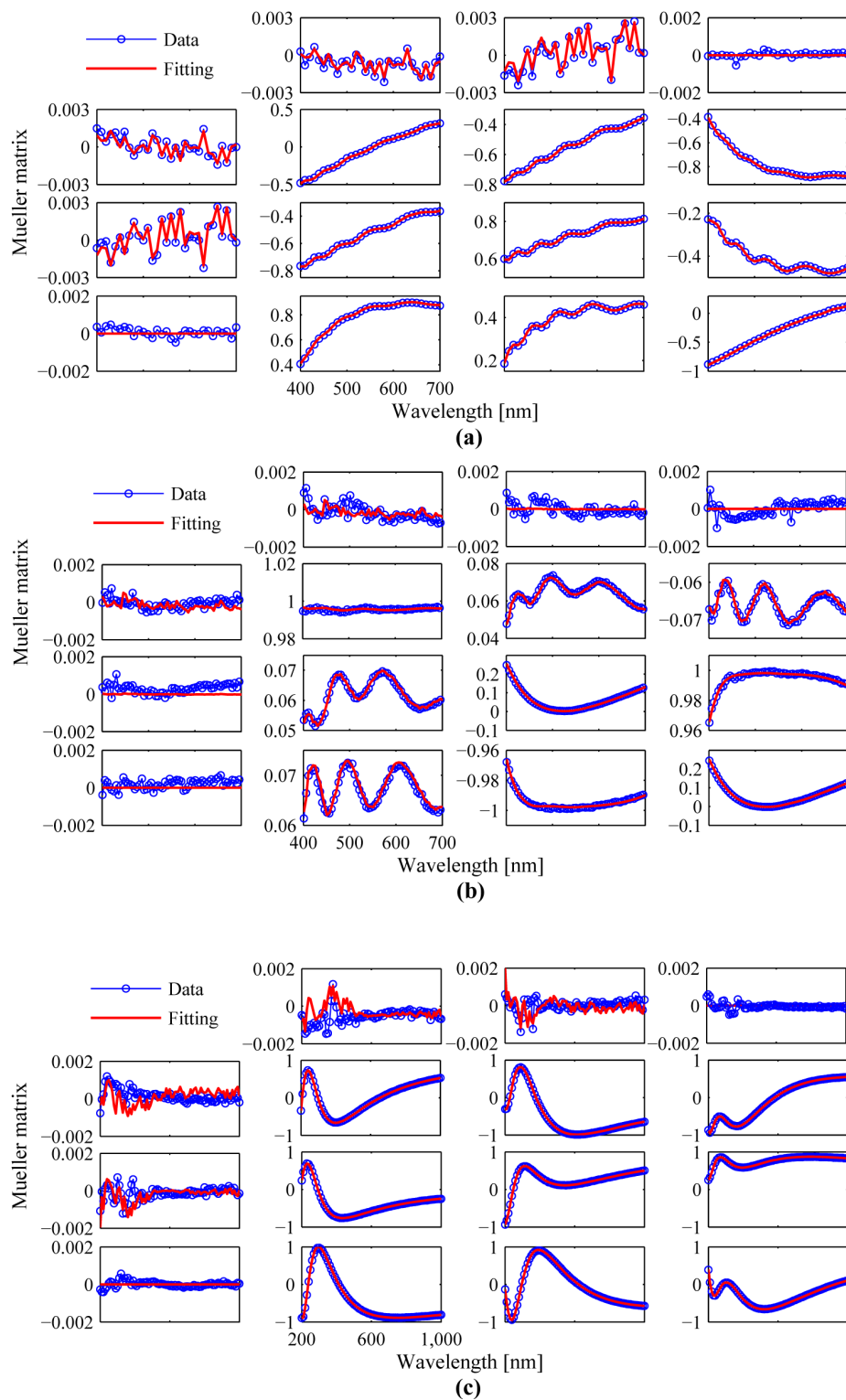


Fig. 3. Mueller matrix spectra: (a) the quartz compound zero-order waveplate; (b) the MgF<sub>2</sub>-MgF<sub>2</sub>-quartz achromatic waveplate; (c) the MgF<sub>2</sub> biplate.

Figure 3(a)–3(c) (the blue solid lines marked with open circles) present the measured Mueller matrix spectra of CW1–CW3, respectively. Since the central wavelength or the applicable wavelength range for the quartz compound zero-order waveplate and the MgF<sub>2</sub>-MgF<sub>2</sub>-quartz achromatic waveplate lies in the visible range, only results over the wavelength range of 400–700 nm are given for these two CWs. As for the MgF<sub>2</sub> biplate, the measured results over the whole spectral range are presented here. From these results, it can be seen that main features of the Mueller matrices are in the bottom-right  $3 \times 3$  matrix blocks, which are mainly determined by the retardance, the fast axis azimuth, and the rotation angle of the waveplates. While the elements in the first row and the first column, especially  $m_{14}$  and  $m_{41}$ , are close to 0. According to Eq. (8), these elements are mainly affected by the diattenuation, and they should be 0 for an ideal waveplate since the diattenuation angle is 45°. Besides, the elements  $m_{14}$  and  $m_{41}$  in the Mueller matrix of a waveplate should be constantly equal to 0, and the data in these positions shown in Figs. 3(a)–3(c) reflects the level of noises and errors of the house-developed MMP system, which is less than 0.2% over the whole spectral range.

#### 4.2 Polarization properties

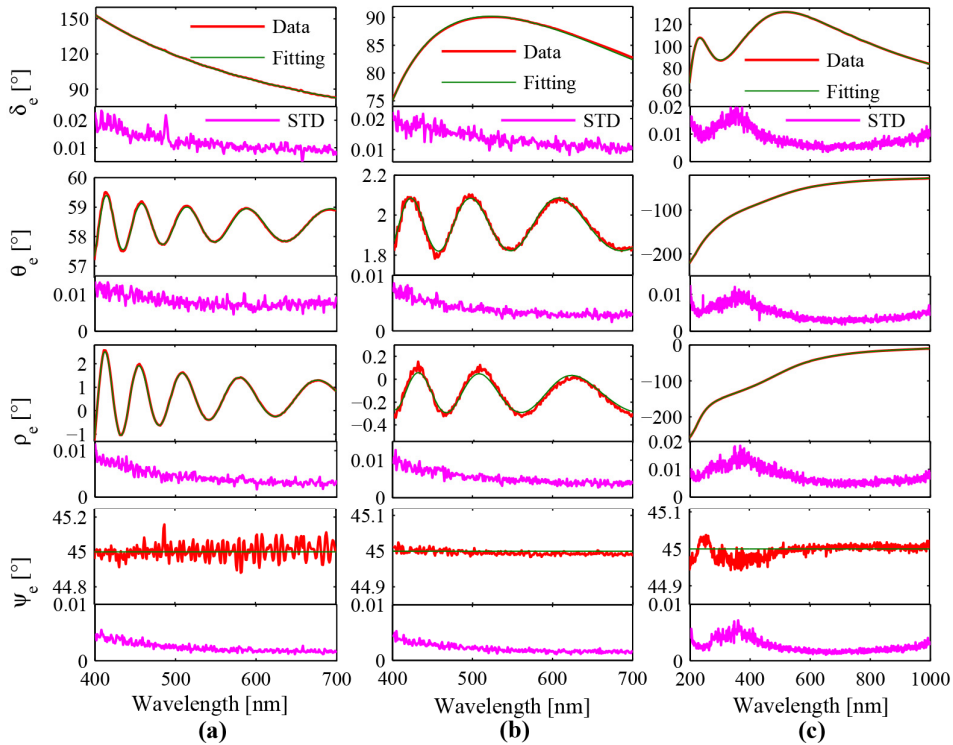


Fig. 4. Spectra for the equivalent polarization parameters over concerned wavelength ranges and their corresponding standard deviations (STD) for 30 repeated measurements: (a) the quartz compound zero-order waveplate; (b) the MgF<sub>2</sub>-MgF<sub>2</sub>-quartz achromatic waveplate; (c) the MgF<sub>2</sub> biplate.

According to the method proposed in Sec. 2, all the equivalent polarization parameters, including the retardance, the fast axis azimuth, the rotation angle, and the diattenuation angle, of the waveplate can be robustly extracted from its measured Mueller matrix spectra. The theoretically calculated Mueller matrix of the best fitting results also have been correspondingly shown in Figs. 3(a)–3(c) (the red solid lines). It can be seen that the best fitting results exhibit extremely high agreement with the measured data. The residual

difference between the measured and the best fitting Mueller matrices may be attributed to the measurement errors and the deflection in the waveplates, such as the depolarization artifacts resulted from the finite bandwidth of the polarimeter [43]. Figures 4(a)–4(c) (the red solid lines) present the extracted results of equivalent polarization parameters for CW1–CW3 over the corresponding spectral ranges, respectively.

It can be seen from Fig. 4(a) that the retardance of the quartz compound zero-order waveplate decreases with the wavelength, which is due to the dispersive characteristics of the birefringence of the quartz crystal. The  $90^\circ$  (i.e., quarter-wave) retardance appears at the wavelength of about 645 nm, which is a little larger than the designed central wavelength of 632.8 nm. And at the designed central wavelength, the measured retardance is about  $91.8^\circ$ , which has a relative error of about  $\lambda/200$  compared with the designed value  $90^\circ$ . The quartz compound zero-order waveplate is designed as a linear retarder, thus the rotation angle should be 0, and the fast axis azimuth should keep a constant over the spectral range. However, it can be observed that the equivalent fast axis azimuth and the equivalent rotation angle exhibit quasi-periodic oscillations. These oscillations can be assigned to the axis alignment errors between the two multi-order single waveplates. Our previous publications [44,45] as well as other researchers' works [15,46,47] have clearly addressed the mechanism and application of this kind of oscillations in calibrating the axis alignment errors and in aligning the fast axes of a CW. Besides, it can be seen that the diattenuation angle spectrum also exhibits obvious oscillations deviating from the ideal value of  $45^\circ$ . Different from the low-frequency but relative large-amplitude oscillations in the fast axis azimuth and the rotation angle, the oscillations in the diattenuation angle spectrum appear with much higher frequency and smaller amplitude. In general, the multiple reflections between the plate planes will result in high-frequency interference ripple in the polarization spectra of the composite waveplate [40,48]. Since the CWs used in this paper were produced with anti-reflection coatings on both sides, the strength of the multiple reflections will be significantly weakened. Based on the above considerations, the relative high-frequency but small-amplitude oscillations in the diattenuation angle are most likely due to multiple reflections, rather than the axis alignment errors. Actually, these high-frequency but small-amplitude oscillations exist in all the polarization parameters of the CW. They appear most clearly in the diattenuation angle just owing to its wavelength independence in the absence of errors. It should be noted that the air-gap structure makes the oscillations resulted from multiple reflections in the quartz compound zero-order waveplate more obvious than those in the other two CWs as discussed later.

From Fig. 4(b), it can be seen that the retardance of the  $\text{MgF}_2\text{-MgF}_2\text{-quartz}$  achromatic waveplate first increases and then decreases with the wavelength in the spectral range of interest. The retardance has a maximum deviation of  $4.7^\circ$  from  $90^\circ$  and remains in the range of about  $85.3^\circ\text{--}90.2^\circ$  over its designed applicable wavelength range of 450–650 nm, which demonstrates that it is a quasi-achromatic quarter-wave retarder. Again we can observe obvious quasi-periodic oscillations in the spectra of the fast axis azimuth and the rotation angle due to the alignment errors between the single waveplates. The deviations in the diattenuation angle of the  $\text{MgF}_2\text{-MgF}_2\text{-quartz}$  achromatic waveplate are much smaller than those of the quartz compound zero-order waveplate. This is because the single waveplates of the achromatic waveplate are cemented together using the glue which has a matched refractive index with those of  $\text{MgF}_2$  and quartz. The matched refractive indices between the glue and the single waveplates reduce the interference effects to a certain degree. Despite this, the interference effect is inevitable, and the high-frequency systematic deviations resulted by the interference effect still exist in the measured spectra.

From Fig. 4(c), we can see that the retardance spectra of the  $\text{MgF}_2$  biplate has two humps, and it remains in the range of  $65.9^\circ\text{--}131.5^\circ$  over the ultra-wide spectral range of 200–1000 nm. Therefore this specially designed  $\text{MgF}_2$  biplate can be used as the polarization modulator for the broadband rotating-compensator polarimetric systems [2]. Significantly different from the former two CWs, the fast axis azimuth and the rotation angle of the  $\text{MgF}_2$  biplate vary within

an ultra-wide range of hundreds of degrees over the whole spectra. These characteristics are due to the specific structure of the  $\text{MgF}_2$  biplate as described in Sec. 3.2 and indicate that it is no longer a linear retarder but instead of a general elliptical retarder. Since the single waveplates directly contact each other without any air gap by using the optical cement method, the deviations in the diattenuation angle are inhibited within a negligible level. The relative larger fluctuations in the diattenuation angle spectrum over the lower wavelengths may be resulted from the imperfections of the material, such as dichroic artifacts. In the ultraviolet range, the deflection in birefringent material and other error sources increase, which result in the relative uneven curves of the measured polarization parameters. Actually, this phenomenon not only exists in  $\psi_e$ , but also exists in all the other parameters. It appears most clearly in  $\psi_e$  just owing to its wavelength independence in the absence of errors.

To further check the measurement precision of the proposed method, 30 repeated measurements have been performed on each of the three CWs. The standard deviations (STD) of the 30 repeated measurements for the polarization parameters of the CWs have been presented in the corresponding bottom subfigures in Fig. 4 (pink solid line). It can be seen that the STD is less than  $0.03^\circ$  for all these polarization parameters over the corresponding wavelength ranges of interest. Theoretically, the measurement precision for the polarization parameters can be evaluated using the measurement precision of Mueller matrix by error propagation formula according to Eq. (9) [49]. Since the measurement accuracy and precision of the MMP are better than 0.2% and 0.1% respectively over the whole spectra range [2], the measurement precision for the polarization parameters should be better than  $0.05^\circ$ , which is consistent with the experimental results. The results indicate that the proposed method has an acceptable and comparable precision with those of most of the existing techniques ranging from less than  $0.01^\circ$  to larger than  $0.5^\circ$  [17].

Results in Figs. 4(a)–4(c) demonstrate that without exception these three practical CWs exhibit both linear retardances and circular retardances, although some of them are designed to be linear retarders. Figure 5 presents the spectra of the elliptical retardances and the ellipticities of the CWs calculated from their measured linear retardances and rotation angles (i.e., circular retardances) according to Eqs. (10) and (11). It can be observed that the quartz compound zero-order waveplate and the  $\text{MgF}_2$ - $\text{MgF}_2$ -quartz achromatic waveplate exhibit small ellipticities with the elliptical retardances mainly contributed by the linear retardances. While the  $\text{MgF}_2$  biplate exhibits a large ellipticity with the elliptical retardance coming from both the linear retardance and the circular retardance. These results confirm the truth that the former two CWs are designed as linear retarders while the  $\text{MgF}_2$  biplate is a general elliptical retarder.

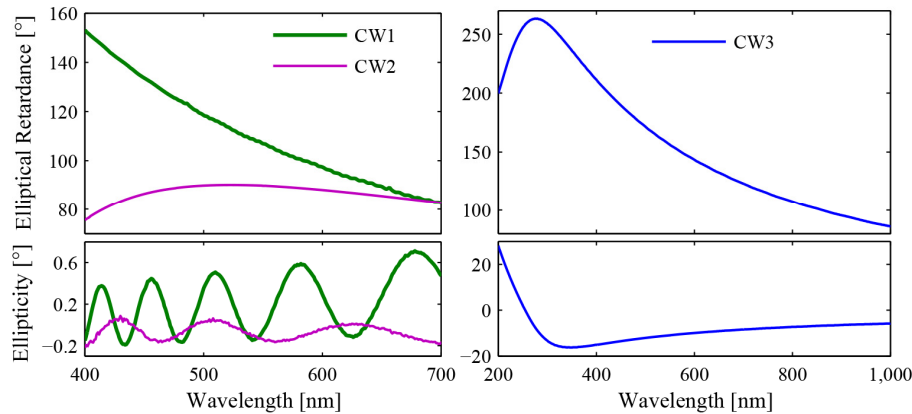


Fig. 5. Elliptical retardances and ellipticities of the tested CWs.

The ellipticity of a CW is determined by the structure of the single waveplates. For a compound zero-order waveplate or a Bechers achromatic waveplate [42], the single waveplates are arranged with their fast axes perpendicular to or parallel with each other to obtain a linear retarder. In this case, the waveplate will exhibit no ellipticity and the fast axis azimuth should remain a constant over the whole spectra. However, inevitable axis alignment errors between the single waveplates make a practical waveplate exhibit small ellipticity oscillating with the wavelength, just like the quartz compound zero-order waveplate and the MgF<sub>2</sub>-MgF<sub>2</sub>-quartz achromatic waveplate tested in this work. For other cases, the single waveplates are arbitrarily arranged to design specific polarization elements for some certain applications, such as the MgF<sub>2</sub> biplate reported in this paper, or some novelly designed CWs. The general structure makes the CW exhibit large ellipticity since it can be optically equal to a cascaded system of a linear retarder and a circular retarder.

It can be concluded that by using the proposed method and the MMP-based experimental set-up, the polarization properties of an arbitrary CW can be comprehensively characterized. All the polarization parameters, including the retardance, the fast axis azimuth, the rotation angle, and the diattenuation angle, can be simultaneously obtained over an ultra-wide spectral range through only one measurement. Besides this, the ellipticity of the CW also can be evaluated and discussed. Based on these polarization spectra, some advanced information about the types, the structures, the applications, as well as the cemented technologies of the CW can be judged or suggested, which is very important for the manufacture and applications of a CW.

#### 4.3 Structure reconstruction

The retardances of the CWs can be calculated with their designed structure parameters and the dispersion equations of MgF<sub>2</sub> and quartz [50,51]. Figure 6 demonstrates the designed spectral curves of the retardances compared with the measured data, and the differences between them are also given in the bottom subfigures. It can be seen that there are systematic deviations in the measured retardances from their designed values. These systematic deviations in the retardances are mainly resulted from the errors in the structure parameters of the CWs, including the errors in the thicknesses of the single waveplates and the alignment errors between the fast axes.

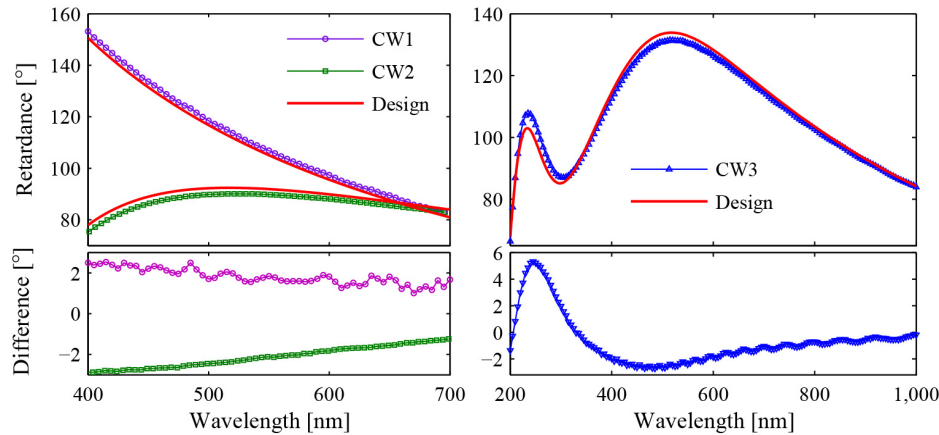


Fig. 6. Designed and measured retardance spectra for the tested CWs.

As proposed in Sec. 2, the practical structure parameters of these CWs can be accurately determined by fitting the measured spectral curves of the equivalent polarization parameters. The best fitting results (green solid lines) have been presented in Figs. 4(a)–4(c) compared

with the measured spectra, and the corresponding structure parameters as well as their  $2\sigma$  standard deviations (STD) of 30 repeated measurements with 95% confidence limits have been given in Table 1 compared their designed nominal values. In the fitting models of these CWs, the diattenuation is neglected. The best fitting results show high agreement with the experimental spectra of the equivalent polarization parameters, and the structure parameters are consistent with their designed values. Besides, the determined global orientations of the CWs (i.e., the fast axis azimuths of the first single waveplates) also agree with the setting values in the experiments as described in Sec. 3.2. There are small axis alignment errors between the single waveplates as shown in Table 1, and that is why the fast axis azimuths and the rotation angles in Figs. 4(a) and 4(b) oscillate with the wavelengths. From these results, we can see that not only the thicknesses and fast axis azimuths of the single waveplates, but also the global orientations and the axis alignment errors can be determined. With these parameters, the actual structures of the CWs can be completely reconstructed, which is extremely useful for processing control, installation, and adjustment, as well as error analysis in manufacturing and implementation. It can be observed that the  $2\sigma$  STDs for the thickness and the azimuth angle are less than 0.15  $\mu\text{m}$  and 0.02° respectively.

**Table 1. Structure parameters of the CWs tested in this paper.**

CW	Thickness (nm)			Fast axis azimuth (°)			Alignment error (°) <sup>b</sup>	
	$d_1$	$d_2$	$d_3$	$\theta_1$ <sup>a</sup>	$\theta_2$	$\theta_3$	$\alpha_1$	$\alpha_2$
1	Nominal	401.50	384.00	—	60	60 + 90	—	0
1	Measure d	$422.21 \pm 0.146^{\text{c}}$	$404.43 \pm 0.122$	—	$58.39 \pm 0.004$	$147.84 \pm 0.006$	—	$0.55 \pm 0.006$
2	Nominal	419.00	200.00	267.50	0	0 + 90	0 + 90	0
2	Measure d	$414.52 \pm 0.115$	$195.80 \pm 0.128$	$267.48 \pm 0.063$	$2.09 \pm 0.003$	$92.08 \pm 0.003$	$91.96 \pm 0.003$	$0.01 \pm 0.002$
3	Nominal	5.36	20.03	—	110	$110 + 45$	—	0
3	Measure d	$5.64 \pm 0.072$	$19.93 \pm 0.120$	—	$106.44 \pm 0.008$	$151.57 \pm 0.012$	—	$0.13 \pm 0.012$

<sup>a</sup>  $\theta_1$  is chosen as the global orientation of the CW;

<sup>b</sup> The alignment error refers to the error in the intersection angle between the fast axes of the single waveplates;

<sup>c</sup> The “ $\pm$ ” refers to the  $2\sigma$  standard deviations (with 95% confidence limits) of 30 repeated measurements.

It should be noted that only the effective thicknesses and fast axis azimuths of the two compound zero-order waveplates and one alignment error between their effective fast axes are fitted and given in Table 1 for the MgF<sub>2</sub> biplate. Actually, the MgF<sub>2</sub> biplate consists of four multi-order single waveplates (i.e., each compound zero-order waveplate contains two multi-order single waveplates). Thus, at least four thicknesses, four fast axis azimuths, and three axis alignment errors should be included in the fitting model for the practical MgF<sub>2</sub> biplate. However, such a model is too complicated and discussing the structure of such a complicated waveplate is beyond the scope of this paper. It can be observed from Fig. 4(c) that the best fitting curves agree very well with the measured spectra, demonstrating that the simplified model used in the fitting is enough to describe the intrinsic features of the MgF<sub>2</sub> biplate.

## 5. Conclusion

In summary, we proposed a MMP-based method for the comprehensive characterization of an arbitrary CW. An analytical model is established to describe a general CW by extending the Jones' equivalent theorem with the Mueller matrix calculus. In the model, four equivalent polarization parameters including the retardance, the fast axis azimuth, the rotation angle and the diattenuation angle, are involved to completely describe the polarization properties of a general practical CW. Relations between the polarization properties, the structure, and the Mueller matrix of the CW are derived. Two regressive procedures are proposed to robustly extract the polarization parameters from the measured Mueller matrix spectra and to further reconstruct the actual structure of the CW. Three typical CWs, including a quartz compound zero-order waveplate, an MgF<sub>2</sub>-MgF<sub>2</sub>-quartz achromatic waveplate, and a specially designed MgF<sub>2</sub> biplate are tested on a house-developed broadband MMP as examples to verify the proposed method. Experimental results and discussions demonstrate that

- (1) The polarization properties of CWs benefit from the proposed method and the full Mueller matrix spectra, and can be comprehensively characterized over an ultra-wide spectral range through only one measurement.
- (2) The actual structure, including the thicknesses and the fast axis azimuths of the single waveplates, the axis alignment errors between the single waveplates, as well as the global orientations of the CWs, can be completely reconstructed.
- (3) Based on these polarization properties and the structures, some advanced information about the types, the applications, the manufacture technologies, and some defect artifacts of these CWs can be studied and discussed.

The methods and results, as well as the discussions reported in this paper are expected to provide some useful knowledge and advice for the control and analysis of an arbitrary CW in the manufacture processing and the applications.

## Funding

National Natural Science Foundation of China (Grant Nos. 51727809, 51805193, 51525502, 51775217); China Postdoctoral Science Foundation (Grant Nos. 2016M602288 and 2017T100546); National Science and Technology Major Project of China (Grant No. 2017ZX02101006-004); National Science Foundation of Hubei Province of China (Grant Nos. 2018CFB559, 2018CFA057).